13. P. Delaney *et al.*, *Nature* **391**, 466 (1998).
14. J. Meyer and G. Minnigerode, *Phys. Lett. A* **38**, 529 (1972).
15. R. Fazio, F. W. J Hekking, A. A. Odintsov, *Phys. Rev. B* **53**, 6653 (1996).
16. D. L. Maslov, M. Stone, P. M. Goldbart, D. Loss, *ibid.*, p. 1548.
17. D. Loss and T. Martin, *ibid.* **50**, 12160 (1994).
18. A. Yu. Kasumov *et al.*, unpublished data.
19. We acknowledge A. Loiseau for collaboration with the preparation of SWNTs on TEM grids and A. MacFarlane for useful comments on the manuscript. We also benefited from fruitful discussions with M. Dévoret, D. Estève, C. Urbina, T. Giamarchi, H. Pothier, and H. Raffy. A.K. thanks The Russian Foundations for Basic Research (grant no. 97-1061) and Solid-State Nanostructures (99-02-1061) for financial support.

31 December 1998; accepted 26 April 1999

A Post-Stishovite SiO_2 Polymorph in the Meteorite Shergotty: Implications for Impact Events

T. G. Sharp,[1]* A. El Goresy,[2]† B. Wopenka,[3] M. Chen[4]

Transmission electron microscopy and electron diffraction show that the martian meteorite Shergotty, a shocked achondrite, contains a dense orthorhombic SiO_2 phase similar to post-stishovite SiO_2 with the α-PbO_2 structure. If an SiO_2 mineral exists in Earth's lower mantle, it would probably occur in a post-stishovite SiO_2 structure. The presence of such a high-density polymorph in a shocked sample indicates that post-stishovite SiO_2 structures may be used as indicators of extreme shock pressures.

The SiO_2 polymorph stishovite forms at high pressure (*1*), and has been found in highly shocked rocks (*2*). The existence and stability of post-stishovite silica (SiO_2 polymorphs denser than stishovite) have been the subject of many recent studies (*3*–*14*). Post-stishovite silica plus magnesiowüstite might be stable relative to (Mg.Fe)SiO_3-perovskite in Earth's lower mantle (*13*, *15*–*17*). Such an SiO_2 phase in heavily shocked samples would also provide a tool for understanding impact processes. Here we describe a post-stishovite SiO_2 phase in the martian meteorite Shergotty.

Shergotty is heavily shocked; it contains maskelynite (*18*–*20*), which was long thought to be diaplectic plagioclase glass that formed by a solid-state transformation (*21*), but appears to have quenched from a shock-induced melt (*22*). Shergotty also contains large silica grains (>150 mm) that were previously interpreted to be birefringent shocked quartz with planar deformation features (*21*). Most are wedge-shaped, which is typical of β-tridymite but atypical of quartz. Like many of the maskelynite grains (*22*), the silica grains lack shock-induced intragranular fractures. Many of the SiO_2 grains are surrounded by radiating cracks (Fig. 1A). These cracks are similar to those formed around coesite in high-pressure metamorphic rocks (*23*) and indicate that the volume of the silica phase increased greatly with decompression. Expansion must have occurred when the maskelynite was solid, because the cracks also cut through it (Fig. 1B). The lamellar texture appears as two sets of lamellae of different brightness in field-emission scanning electron microscopy images recorded in back-scattered-electron (BSE) mode (Fig. 1B). Electron microprobe (EMP) analyses of the largest lamellae (up to several micrometers wide), using a slightly defocused electron beam, revealed that both the bright and dark lamellae are SiO_2 compounds that are identical in composition and have minor concentrations of Na_2O (0.4% by weight) and Al_2O_3 (1.12%). BSE imaging with a field-emission scanning electron microscope (FESEM) at low accelerating voltages revealed that the original silica grains consist of a mosaic of many individual domains (10 to 50 μm in diameter), each with a distinct pattern of intersecting thin (<300 nm) lamellae (Fig. 1B).

We investigated the crystallinity and structure of SiO_2 phases using laser Raman microprobe spectroscopy, transmission electron microscopy (TEM), and selected-area electron diffraction (SAED). Three zone-axis SAED patterns (Fig. 2) were collected from a domain of crystalline material. These patterns all show sharp intensity maxima and diffuse rings, corresponding to diffraction from the crystalline material and diffuse scattering from amorphous material, respectively. Starting from zone axis 1 (Fig. 2A), the crystal was tilted 21° about the vertical diffraction vector (with d spacing = 4.54 Å) to reach zone axis 2 (Fig. 2B). The reflection corresponding to 4.54 Å disappeared as the sample was tilted out of zone axis 1 and remained absent in zone axis 2, indicating that it is a forbidden reflection that occurs by dynamical diffraction in zone axis 1. Zone axis 3 (Fig. 2C) was reached by tilting the crystal 37° from zone axis 1 about the horizontal diffraction vector (d = 3.22 Å). In this case, the d = 3.22 Å reflection remained excited and therefore is not forbidden. The three zone axis patterns contain seven diffraction vectors that can be used to constrain the structure of this SiO_2 polymorph.

The diffraction data (Fig. 2) cannot be indexed using the structures of SiO_2 polymorphs that are stable at low pressures. Although tridymite is a likely SiO_2 phase in Shergotty before shock metamorphism, the diffraction data are inconsistent with all tridymite polymorphs (*24*). Similarly, the diffraction data are inconsistent with coesite and stishovite. The data are also inconsistent with known post-stishovite structures, including the $CaCl_2$, baddelyite, and α-PbO_2, and modified baddelyite (*Pnc*2) structures of SiO_2. The diffraction data from zone axis 1 fit a post-stishovite structure with space group *Pbcn* that is similar to the α-PbO_2 structure (*25*-*27*), but the d spacings from zone axes 2 and 3 fit less well to this α-PbO_2–like structure (*27*). Our data also nearly fit a $Pca2_1$ structure calculated to be a quench phase from post-stishovite SiO_2 at 50 GPa and a 10-GPa differential stress (*28*). The cell parameters of $Pca2_1$ and *Pbcn* structures are nearly the same, but they do not match the 1.97 Å and 3.41 Å d spacings of our data (Table 1).

Because the symmetries of our diffraction patterns are consistent with an orthorhombic lattice and the reflections can be indexed to *Pbcn* and $Pca2_1$ structures (*27*, *28*), we refined new orthorhombic cell parameters to fit our data (Table 1). All our d-space data fit the refined orthorhombic unit cells within 1% (Ta-

Table 1. d-space data obtained from the three zone-axis diffraction patterns as compared to calculated d spacings for *Pbcn* and $Pca2_1$ SiO_2 structures (*27*, *28*) and the refined unit cells based on the *Pbcn* structure. Miller indices (*hkl*) are also given for each structure, with an asterisk indicating the reflections that are forbidden

SAED	*Pbcn*		$Pca2_1$		Refined *Pbcn*	
4.54*	001*	4.50	100*	4.49	001*	4.55
3.41	011*	3.25	110	3.25	011*	3.40
3.22	110	3.17	011*	3.17	110	3.23
3.09	101*	3.11	101*	3.11	101*	3.07
2.62	111	2.59	111	2.59	111	2.63
2.28	002	2.25	200	2.25	002	2.28
1.97	121	1.88	121	1.88	121	1.97

[1]Department of Geology, Arizona State University, Tempe, AZ 85287, USA. [2]Max-Planck-Institut für Kernphysik, Post Office Box 103 980, 69029 Heidelberg, Germany. [3]Department of Earth and Planetary Sciences, Washington University, St. Louis, MO 63130, USA. [4]Guangzhou Institute of Geochemistry, Academie Sinica, Guangzhou 510640, China.

*To whom correspondence should be addressed.
†Present address: Max-Planck-Institut für Chemie, J.-Becher-Weg 27, 55128 Mainz, Germany.

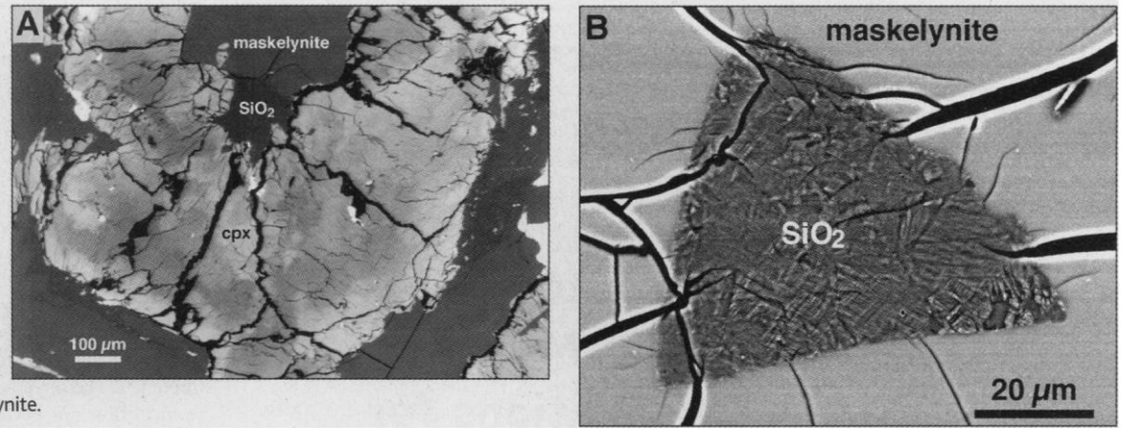

Fig. 1. BSE-mode SEM images of SiO_2 and maskelynite. (**A**) An SiO_2 grain and maskelynite are surrounded by a fractured clinopyroxene (cpx) where the fractures radiate more than 500 μm from the SiO_2. (**B**) FESEM image of a triangular SiO_2 grain showing the tweedlike internal microstructure with some nearly orthogonal lamellae and fractures radiating outward into the surrounding maskelynite.

ble 1). Our diffraction data also fit both refined lattices in terms of interplanar angles and angles between zone axes. Many forbidden reflections that are expected for the *Pbcn* and $Pca2_1$ space groups (Table 1) are present in our diffraction patterns as a result of dynamical diffraction effects. However, the 3.22 Å reflection (011 in $Pca2_1$) is not extinct as it would be for $Pca2_1$ ($0kl$, $l = 2n$). A monoclinic structure ($P2_1$, a = 4.58 Å, b = 4.17 Å, c = 5.13 Å, and β = 88.85°) has been calculated (*28*) that also fits our refined lattice parameters, but the extinct 4.54 Å reflection (100 in $P2_1$) is not forbidden for this structure. Although our diffraction data are insufficient to determine the space group, they fit an orthorhombic unit cell (a = 4.16 ± 0.03 Å, b = 5.11 ± 0.04 Å, c = 4.55 ± 0.01 Å, cell volume V = 96.91 ± 0.63 Å^3) and are consistent with the *Pbcn* space group of α-PbO_2. Assuming four formula units per cell as in *Pbcn*, the density is 4.12 gm/cm^3.

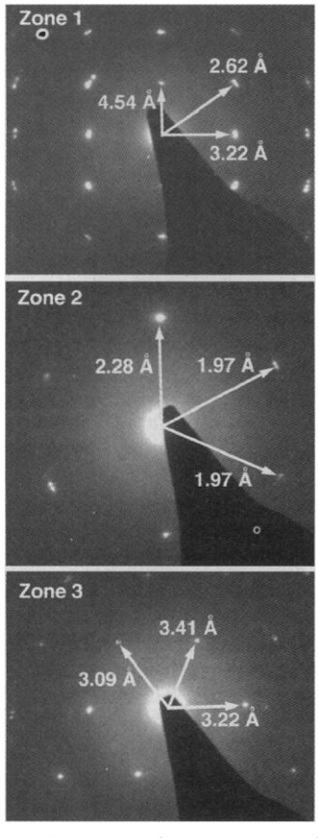

Fig. 2. SAED patterns of three zone axes from a small cluster of crystalline SiO_2. The diffraction vectors are marked by their corresponding d spacings. Although zones 1 and 2 share the same vertical direction in reciprocal space, the 4.54 Å reflection does not appear in zone 2.

The electron diffraction (Figs. 2 and 3) and bright-field imaging (Fig. 3) data also show that some of the SiO_2 is amorphous. This material produces a diffuse diffraction ring (Fig. 2), whereas the crystalline material produces discrete sharp reflections. In the bright-field image (Fig. 3), the strongly diffracting crystalline material appears darker than the amorphous SiO_2. The crystalline grains are 50- to 200-nm-wide islands embedded in 50- to 100-nm-wide amorphous veins (Fig. 3) that are similar in size to the fine features observed in the FESEM images (Fig. 1B). Many of the amorphous veins are parallel to (001) (using *Pbcn*) or subparallel to (110) (Fig. 3).

The tweedlike microstructure in the silica grains of Shergotty is not the result of shock-induced vitrification of quartz, as previously interpreted (*21*), but rather represents the post-shock vitrification of unstable SiO_2 polymorphs formed during shock. The orthogonal lamellae seen in BSE images correspond to amorphous veins and intergrowths of crystalline SiO_2 polymorphs (*26*). BSE images (Fig. 1B) also show domains with nearly constant lamellae orientations that may represent single crystals of high-pressure SiO_2 in a larger polycrystalline SiO_2 grain.

Laser Raman microprobe (LRM) analysis of optically visible SiO_2 lamellae does not show evidence for the presence of known low- or high-pressure crystalline SiO_2 polymorphs. Instead, the spectrum (Fig. 4) appears to be that of a high-density glass (*29–31*) similar to silica glass quenched from 30 GPa (*31*), but could presumably also be that of a mixture of dense vitreous and crystalline SiO_2. There are several possible reasons for the lack of spectral features indicative of crystalline SiO_2: (i) the crystalline SiO_2 polymorph may not have a (strong) Raman spectrum, (ii) the volume concentration of the crystalline phase within the irradiation volume is too small, (iii) the selection rules for the vibrational spectrum of the crystalline SiO_2 phase break down because of its small crystallite size, or (iv) the crystalline material is unstable under the laser beam and vitrifies during acquisition of the Raman spectrum. The last explanation is likely because of the unstable nature of the SiO_2 in Shergotty (*32*).

The SiO_2 was extremely sensitive to irradiation damage during TEM and rapidly became amorphous even with low electron doses (*32*). The SiO_2 was much less stable than synthetic stishovite previously analyzed (*33*, *34*). The extreme instability of the crystalline SiO_2 is consistent with the new orthorhombic structure being a dense silica polymorph. The observation that this highly unstable phase has survived the post-shock thermal history of Shergotty suggests that the post-shock temperatures of the meteorite were relatively low [see also (*35*, *36*)].

Theoretical calculations and diamond-anvil experiments demonstrate that stishovite ($P4_2/mnm$) transforms into the $CaCl_2$ structure by a displacive mechanism at pressures above about 45 GPa, but the SiO_2 polymorphs that are stable at higher pressures are controversial (*10*, *11*). The following sequence of SiO_2 phase transitions has been proposed (*10*): stishovite ($P4_2/mmm$) → $CaCl_2$ (*Pnnm*) → modified baddelyite (*Pnc*2) → pyrite (*Pa*3). Dubrovinsky *et al.* (*10*) argue that the *Pnc*2 structure, intermediate between that of α-PbO_2 and baddelyite, is the stable polymorph at pressure (P) > 80 GPA, whereas Teter *et al.* (*11*) argue that the α-PbO_2 structure is stable above 80 GPa; the structures and total energies of *Pnc*2 and α-PbO_2 SiO_2 phases are similar (*11*). Our SiO_2 structure is distinctly different from the α-PbO_2 and *Pnc*2 structures but similar to a *Pbcn* structure produced

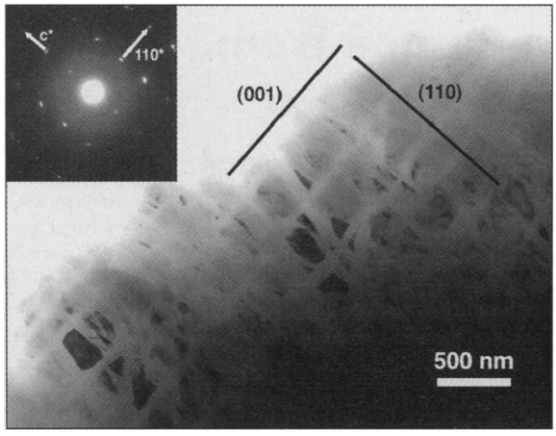

Fig. 3. Bright-field TEM image of SiO_2 showing dark islands of crystalline material (strongly diffracting) cut by numerous veins of lighter contrast amorphous material. The SAED pattern shows the [$\bar{1}$10] zone axis of the SiO_2 polymorph (based on the *Pbcn* setting) with a faint diffuse ring representing diffuse scattering by the amorphous veins. The amorphous veins occur predominantly parallel to (001) and subparallel to (110).

in shock experiments at 70 to 90 GPa (*27*) and a quench phase from diamond anvil experiments done without a pressure medium (*6*). The similarity between our orthorhombic phase, the phase created by Tsuchida and Yagi (*6*), and structures calculated to quench from 50 GPa and a differential stress of 10 GPa (*28*) suggest that the SiO_2 phase in Shergotty may have been stabilized by high differential stress rather than pressures in excess of 80 GPa.

The presence of Na_2O and Al_2O_3 in the SiO_2 grains, and their morphology, are consistent with the low-pressure precursor phase having been tridymite. The maskelynite and silica apparently melted during shock and solidified under high pressure. However, the abrupt contacts between angular SiO_2 grains and surrounding maskelynite (Fig. 1B), and the morphology of the silica grains (Fig. 1B), are inconsistent with both phases being liquids simultaneously. We have observed limited mixing of SiO_2 and maskelynite along some grain margins as well as textures suggesting injection of SiO_2 into fractures. We conclude that the post-stishovite SiO_2 formed primarily by a solid-state transformation and to a lesser extent by melting and subsequent crystallization.

The presence of post-stishovite SiO_2 in Shergotty implies that the inferred 29-GPa shock pressure (*21*) is too low, and the shock pressure probably exceeded the stability range of stishovite (>45 GPa). The new polymorph cannot have formed through decompression of the $CaCl_2$ structure because the latter is unquenchable and inverts to stishovite upon decompression (*8–11*). Instead, it is likely to be a quench product from a post-stishovite structure such as α-PbO_2. The maximum shock pressure is uncertain. In some experiments extensive melting and extreme shock deformation take place in excess of 80 GPa (*37*), whereas experiments on chondritic samples up to 83 GPa show little melting (*38–40*). The disparity between the 29-GPa and the >80-GPa pressure implied by α-PbO_2–like SiO_2 cannot be resolved until more is known about the stability of these phases and the role of differential stress in post-stishovite–SiO_2 phase transitions.

The stability of (Mg,Fe)SiO_3-perovskite in the deep lower mantle is dependent on the structures and free energies of the SiO_2 phases. If (Mg,Fe)SiO_3-perovskite decomposes to SiO_2 plus magnesiowüstite in the lower mantle (*16–17*), the SiO_2 would have a post-stishovite structure. The present results confirm the existence of such a structure in a natural sample.

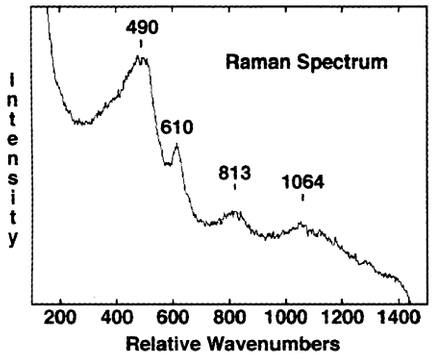

Fig. 4. Bulk Raman analysis of 1- to 2-μm areas in both light and dark lamellae showed no indication of crystalline material.

References and Notes

1. S. M. Stishov and S. V. Popova, *Goekhimiya* **10**, 923 (1961).
2. E. C. T. Chao, J. J. Fahey, J. Littler, D. J. Milton, *J. Geophys. Res.* **67**, 419 (1962).
3. L. Liu, W. A. Basset, J. Sharry, *ibid.* **83**, 2301 (1978).
4. T. Sekine, M. Akaishi, N. Setaka, *Geochim. Cosmochim. Acta* **51**, 379 (1987).
5. Y. Tsuchida and T. Yagi, *Nature* **339**, 209 (1989).
6. ———, *ibid.* **347**, 267 (1990).
7. R. J. Hemley, C. T. Prewitt, K. J. Kingma, in *Silica Physical Behavior, Geochemistry and Materials Applications*, P. J. Heaney, C. T. Prewitt, G. V. Gibbs, Eds. (Mineralogical Society of America, Washington, DC, 1994), vol. 29, pp. 41–73.
8. K. J. Kingma, R. E. Cohen, R. J. Hemley, H.-K. Mao, *Nature* **374**, 243 (1995).
9. A. B. Belonoshko, L. S. Dubrovinsky, N. A. Dubrovinsky, *Am. Miner.* **81**, 785 (1996).
10. L. S. Dubrovinsky *et al.*, *Nature* **388**, 362 (1997).
11. D. M. Teter, R. J. Hemley, G. Kresse, J. Hafner, *Phys. Rev. Lett.* **80**, 2145 (1998).
12. B. B. Karki, M. C. Warren, G. J. Ackland, J. Crain, *Phys. Rev. B* **55**, 3465 (1997).
13. E. Knittle and R. Jeanloz, *Science* **251**, 1438 (1991).
14. T. J. Ahrens, in *Advanced Materials '96*, proceedings of the 3rd National Institute for Research in Inorganic Materials International Symposium on Advanced Materials, Tsukuba, Japan, 4 to 8 March 1996, M. Akaishi *et al.*, Eds. (National Institute for Research in Inorganic Materials, Tokyo, 1996), pp. 1–4.
15. C. Meade, H.-K. Mao, J. Hu, *Science* **268**, 1743 (1995).
16. S. K. Saxena *et al.*, *ibid.* **274**, 1357 (1996).
17. S. K. Saxena, L. S. Dubrovinsky, P. Lasor, J. Hu, *Eur. J. Miner.* **10** 1275 (1998).
18. M. G. Tschermak, *Sitzungsberichte der Matematisch-Naturwissenschaftlichen Classe der kaiserlichen Akademie der Wissenschaften* **LXV**, 122 (1872).
19. J. V. Smith and R. L. Hervig, *Meteoritics* **14**, 121 (1979).
20. E. M. Stolper and H. Y. J. McSween, *Geochim. Cosmochim. Acta* **43**, 598 (1979).
21. D. Stöffler *et al.*, *ibid.* **50**, 889 (1986).
22. A. El Goresy, B. Wopenka, M. Chen, G. Kurat, *Meteoritics* **32**, A38 (1997).
23. P. Gillet, J. Ingrin, C. Chopin, *Earth Planet. Sci. Lett.* **70**, 426 (1984).
24. P. J. Heaney, in *Silica Physical Behavior, Geochemistry and Materials Applications*, P. J. Heaney, C. T. Prewitt, G. V. Gibbs, Eds. (Mineralogical Society of America, Washington, DC, 1994), vol. 29, pp. 1–40.
25. A. El Goresy, T. G. Sharp, B. Wopenka, M. Chen, *Lunar Planet. Sci. Conf.* **XXIX**, 1707 (1998).
26. New data presented in an abstract in 1998 show that some SiO_2 grains contain crystalline lamellae [T. G. Sharp, A. El Goresey, L. Dubrovinsky, M. Chen, *Meteorit. Planet Sci.* **33**, A144 (1998)].
27. V. N. German, M. A. Podurets, R. F. Trunin, *Sov. Phys. JETP* [Zhurnal eksperimental' noi I teoreticheskoi fiziki of the Academy of Sciences of the USSR] **37**, 107 (1973).
28. In collaboration with L. Dubrovinsky, we are calculating possible SiO_2 structures that may be consistent with the SiO_2 structure described here and the quench phases of German *et al.* (*27*) and Y. Tsuchida and T. Yagi (*6*).
29. F. L. Galeener, *J. Non-Cryst. Solids* **49**, 53 (1982).
30. P. McMillan, B. Piriou, R. Couty, *J. Chem. Phys.* **81**, 4234 (1984).
31. R. J. Hemley, H. K. Mao, P. M. Bell, B. O. Mysen, *Phys. Rev. Lett.* **57**, 747 (1986).
32. To avoid analytical artifacts, we studied different lamellae-bearing SiO_2 grains using each of the techniques. The LRM analysis, using a laser of ~3 mW power at the sample surface, was destructive and produced "burn spots" observed in reflected white light after LRM analysis. During EMP analysis, the SiO_2 grains instantaneously expanded and cracked under the focused electron beam, causing the carbon coat to spall off at the area of irradiation. The samples were thinned for TEM by ion milling with a liquid-nitrogen sample stage to reduce sample temperature and prevent thermal decomposition. TEM data were collected with a slow-scan charge-coupled device camera and a very low electron dose. Tilting of the crystal was done in SAED mode with a camera length of 300 mm so that many reflections could be seen even under very low dose conditions.
33. T. G. Sharp *et al.*, *Phys. Chem. Miner.* **23**, 17 (1996).
34. B. Poe, F. Seifert, T. G. Sharp, Z. Wu, *ibid.* **24**, 477 (1997).
35. T. G. Sharp, C. M. Lingemann, C. Dupas, D. Stöffler, *Science* **277**, 352 (1997).
36. N. Tomioka and K. Fujino, *ibid.*, p. 1084.
37. D. Stöffler, A. Bischoff, V. Buchwald, A. E. Rubin, in *Meteorites and the Early Solar System*, J. F. Kerridge and M. S. Mathews, Eds. (Univ. of Arizona Press, Tucson, AZ, 1988), pp. 165–204.
38. D. Bogard, F. Hoerz, P. Johnson, *Geochim. Cosmochim. Acta* **51**, 2035 (1987).
39. R.-T. Schmitt and D. Stoeffler, *Meteorit. Planet. Sci.* **30**, 574 (1995).
40. X. Xie, C. Dai, M. Chen, A. El Goresy, *ibid.* **32**, A143 (1997).

41. Supported in part by the NASA Cosmochemistry Program, grant NRA 97-OSS-04. M.C. was supported by the National Science Foundation of China (NSFC) under grant 49825132.

2 February 1999; accepted 13 April 1999